Published in final edited form as:

Immunity. 2018 August 21; 49(2): 301–311.e5. doi:10.1016/j.immuni.2018.07.005.

Glycan-Masking Focuses Immune Responses to the HIV-1 CD4-Binding Site and Enhances Elicitation of VRC01-Class Precursor Antibodies

Hongying Duan[1,10], **Xuejun Chen**[1,10], **Jeffrey C. Boyington**[1,10], **Cheng Cheng**[1,10], **Yi Zhang**[1], **Alexander J. Jafari**[1], **Tyler Stephens**[2], **Yaroslav Tsybovsky**[2], **Oleksandr Kalyuzhniy**[3,4], **Peng Zhao**[5], **Sergey Menis**[3,4], **Martha C. Nason**[5], **Erica Normandin**[1], **Maryam Mukhamedova**[1], **Brandon Dekosky**[1,6,7], **Lance Wells**[8], **William R. Schief**[3,4], **Ming Tian**[9], **Frederick Alt**[9], **Peter D. Kwong**[1], **John R. Mascola**[1,11,*]

[1]Vaccine Research Center, NIAID, NIH, Bethesda, MD 20892

[2]Electron Microscopy Laboratory, Cancer Research Technology Program, Leidos Biomedical Research, Inc., Frederick National Laboratory for Cancer Research, Frederick, MD 21701

[3]Center for HIV/AIDS Vaccine Immunology and Immunogen Discovery, The Scripps Research Institute, La Jolla, CA 92037

[4]IAVI Neutralizing Antibody Center, The Scripps Research Institute, La Jolla, CA 92037

[5]Biostatistics Research Branch, Division of Clinical Research, NIAID, NIH, Bethesda, MD 20852

[6]Department of Chemical & Petroleum Engineering, The University of Kansas, Lawrence, KS 66045

[7]Department of Pharmaceutical Chemistry, The University of Kansas, Lawrence, KS 66045

[8]Complex Carbohydrate Research Center, University of Georgia, Athens, GA 30602

[9]Boston Children's Hospital and Harvard Medical School, Boston, MA 02115

Summary

[*]Correspondence: jmascola@nih.gov (J.R.M.).
[10]These authors contributed equally.
[11]Lead Contact

Author contributions

H.D., X.C., C.C., J.C.B., and J.R.M. designed the study and analyzed and interpreted data. C.C.; P.D.K., W.R.S., L.W. and J.R.M. oversaw experiments; H.D., X.C., B.D., E.N., M.M., T.S., Y.T., A.J.J., L.W., P.Z., S.M., and O.K. performed experiments; J.C.B. designed glycan mutants; M.T. and F.A. provided the mouse model and reagents for genotyping; H.D. bred, genotyped, characterized and immunized transgenic mice, and performed single-cell PCR and sequence analysis; X.C. expressed and purified all proteins including probes and performed antigenic analysis of eOD-GT8 mutants; H.D. and X.C. sorted B cells, performed serological and splenocyte analysis; Y.Z. and A.J.J. participated in mouse breeding and genotyping; S.M. and O.K. performed SPR experiments and analysis was overseen by W.R.S.; L.W. and P.Z. performed glycan occupancy mass spectrometry analysis; Y.T. and T.S. performed electron microscopy analysis; M.C.N. performed statistical analysis; H.D., X.C., J.C.B. and C.C. drafted the manuscript and J.R.M., P.D.K., W.R.S., F.A., M.T., L.W., P.Z., A.J. and Y.T. contributed to manuscript revision.

Declaration of interests

The authors declare that an intellectual property application, PCT/US2018/024330, has been filed.

An important class of HIV-1 broadly neutralizing antibodies, termed the VRC01-class, targets the conserved CD4-binding site (CD4bs) of the envelope glycoprotein (Env). An engineered Env outer domain (OD) eOD-GT8 60mer nanoparticle has been developed as a priming immunogen for eliciting VRC01-class precursors and is planned for clinical trials. However, a substantial portion of eOD-GT8-elicited antibodies target non-CD4bs epitopes, potentially limiting its efficacy. We introduced *N*-linked glycans into non-CD4bs surfaces of eOD-GT8 to mask irrelevant epitopes and evaluated these mutants in a mouse model that expressed diverse immunoglobulin heavy chains containing human IGHV1-2*02, the germline VRC01 V_H segment. Compared to the parental eOD-GT8, a mutant with five added glycans stimulated significantly higher proportions of CD4bs-specific serum responses and CD4bs-specific immunoglobulin G^+ B cells including VRC01-class precursors. These results demonstrate that glycan-masking can limit elicitation of off-target antibodies and focus immune responses to the CD4bs, a major target of HIV-1 vaccine design.

Graphical Abstract:

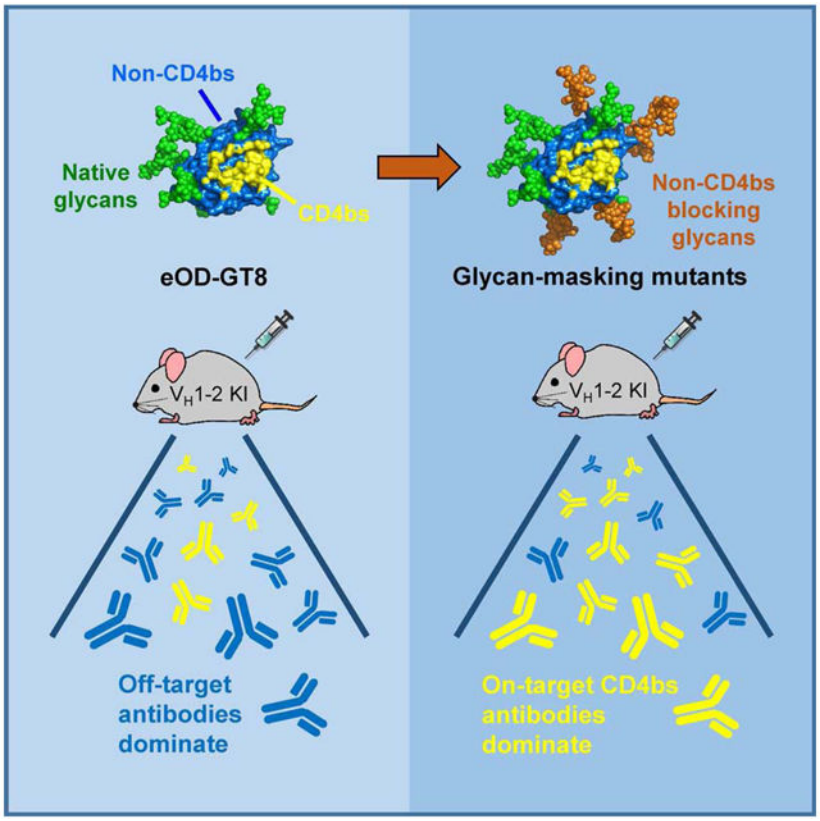

eTOC blurb:

A substantial portion of the engineered HIV gp120 immunogen eOD-GT8-elicited antibodies target non-CD4 binding site (bs) epitopes, potentially limiting its efficacy. Duan et al. used N-linked glycans to mask epitopes outside the CD4bs of eOD-GT8, leading to enhanced elicitation of CD4bs antibodies, including VRC01-class precursors, and reduced off-target antibody responses in a human V_H1-2 mouse model.

INTRODUCTION

The elicitation of protective antibodies against HIV-1 remains a major scientific challenge. While passive administration of HIV-1 specific neutralizing antibodies in animal models can fully protect against infection (Gautam et al., 2016; Julg et al., 2017; Mascola et al., 2000; Nishimura et al., 2017; Saunders et al., 2015), the induction of such antibodies via immunization has not yet been achieved (Burton and Hangartner, 2016; Pegu et al., 2017). Multiple broadly neutralizing antibodies (bNAbs) targeting the CD4-binding site (CD4bs), including VRC01, NIH45-46, VRC-PG04, VRC13, 3BNC117, CH103 and N6, have been isolated from HIV-1 infected individuals and can potently neutralize diverse strains of HIV-1 (Huang et al., 2016; Liao et al., 2013; Scheid et al., 2011; Wu et al., 2010; Wu et al., 2015; Wu et al., 2011; Zhou et al., 2015). Many of these CD4bs-directed human bNAbs share three common characteristics, as typified by the prototype antibody VRC01 and are termed VRC01-class antibodies (Jardine et al., 2016b; Kwong and Mascola, 2012; Scheid et al., 2011; West et al., 2012; Wu et al., 2010; Wu et al., 2011; Zhou et al., 2013): 1) a IGHV1-2 heavy chain, 2) an unusually short 5 amino acid light chain complementarity-determining region 3 (CDRL3) loop, and 3) high levels of somatic hypermutation (SHM).

In contrast to the broad and potent neutralization activity of mature VRC01-class antibodies, inferred VRC01-class unmutated common ancestors (UCA) or germline revertants show little or no detectable interaction with gp120 monomers or native envelope (Env) trimers (Jardine et al., 2013; Hoot et al., 2013; McGuire et al., 2013; Scharf et al., 2013; Zhou et al., 2010). However, engineered gp120 Env or their outer domains (OD) derived from specific HIV-1 strains have been reported to bind VRC01-class germline precursors as well as to activate B cells expressing the corresponding B cell receptors in vitro or in vivo (Jardine et al., 2013; Jardine et al., 2016a; McGuire et al., 2016; McGuire et al., 2013). One such construct, eOD-GT8 60mer, an engineered, circularly permutated OD genetically fused to a 60 subunit self-assembling nanoparticle, binds VRC01-class precursors with high affinity (Jardine et al., 2016a) and has been shown to elicit VRC01-class germline precursors with a 5-amino acid CDRL3 in various IGHV1-2 knock-in mouse models or in immunoglobulin (Ig)-humanized mice (Jardine et al., 2015; Sok et al., 2016; Tian et al., 2016; Abbott et al., 2017). However, eOD-GT8 also possesses significant off-target immunogenicity, as demonstrated by a high titer of immune serum binding to the CD4bs-knock out (KO) eOD-GT8 variant and by a high percentage of antigen-specific B cells reacting to the CD4bs-KO protein (Jardine et al., 2015; Sok et al., 2016; Tian et al., 2016). Such off-target responses may reduce the effectiveness of priming and could present a major challenge for subsequent boost strategies.

One way to mitigate off-target immune responses is to alter the immunogen surface through targeted point mutations and deletions (Dey et al., 2007; Dey et al., 2009; Onda et al., 2008; Wyatt et al., 1993). However, introduction of *N*-linked glycans by means of the NxS/T sequon (Marshall, 1974) to cover irrelevant epitopes, provides a versatile alternative with potentially more predictable outcomes. Prior studies (Ahmed et al., 2012; Forsell et al., 2013; Garrity et al., 1997; Ingale et al., 2014; Lin et al., 2014; Pantophlet et al., 2003, 2004; Sampath et al., 2013; Selvarajah et al., 2005; Selvarajah et al., 2008) involving HIV-1 gp120 core, influenza hemagglutinin or Plasmodium vivax Duffy protein have shown that off-target

antibody responses can be decreased through the introduction of *N*-linked glycans. However, this approach has not yet been employed to focus or enhance the elicitation of a specific class of neutralizing antibodies, such as the VRC01-class bNAbs. To focus the immune responses to the CD4bs, we used structural information to introduce sequons for *N*-linked glycans at 13 different locations on the non-CD4bs surface of eOD-GT8. The antigenic integrity of these glycan-masked variants was verified with VRC01-class bNAbs, their germline revertants and non-CD4bs-specific antibodies. Glycan mutants with high binding to CD4bs-specific antibodies, but reduced binding to non-CD4bs-specific antibodies, were selected and further tested in an IGHV1-2*02 knock-in mouse model. In this model, the knock-in germline human IGHV1-2*02 heavy chain gene segment recombines with mouse D_H and J_H gene segments to generate a diverse repertoire of CDRH3s (Tian et al., 2016) and pairs with the full repertoire of mouse Ig light chains. Here, we demonstrated that glycan-masking of the non-CD4bs surface of eOD-GT8 reduced off-target immune responses and facilitated the elicitation of VRC01-class precursor antibodies.

RESULTS

Design of eOD-GT8 glycan-masking mutants

Despite ten predicted native *N*-linked glycans on the surface of eOD-GT8, a considerable area of protein surface outside the CD4bs is exposed. To reduce off-target immunogenicity of eOD-GT8, we masked non-CD4bs regions from the humoral immune system by introducing *N*-linked glycans onto the OD portion of the eOD-GT8 60mer surface using the crystal structure of the eOD-GT8 monomer (Jardine et al., 2016a) as a model. Thirteen potential sites for the introduction of NxT sequons were identified by using the following criteria: 1) surface residues at least 5Å from the CD4bs, 2) not adjacent to native glycans, 3) NxT mutations not expected to disrupt the structure of eOD-GT8 and 4) high probability of glycosylation as determined from the sequence surrounding the sequon (Figure 1A). NxT sequons were used exclusively as they are glycosylated more efficiently than NxS sequons (Kaplan et al., 1987; Kasturi et al., 1995). Thirteen single glycan mutants, each containing one added glycan, were created for individual evaluation (eOD-GT8-mut1-12 and eOD-GT8-mut23; Figure 1B and Table S1). Structural modeling of the added glycans revealed the extensive non-CD4bs surface that could be covered by these glycan additions (Figure 1C and 1D).

To maximize the masking area while ensuring protein stability, we further designed 35 multi-glycan mutants, each containing two to six of the 13 new glycans (eOD-GT8-mut13-22 and eOD-GT8-mut24-48 in Table S1). As previous studies have suggested that protruding loops tend to be immunogenic (Novotny et al., 1986; Thornton et al., 1986), we focused on such regions of the non-CD4bs surface of eOD-GT8 as potential immunogenic hotspots when creating groupings for glycan-masking. Examination of the eOD-GT8 monomer crystal structure indicated that the glycans from eOD-GT8-mut1, 2, 3, 7, 10 and 11 were each located on protruding loops. Additionally, in three mutants (eOD-GT8-mut24, 27 and 39), we moved the native glycan at 289 to position 287 to improve glycan coverage. Finally, the conserved N276 and N463 glycans existing in over 90% of HIV-1 strains, were also incorporated in eOD-GT8-mut42-48 (Table S1).

eOD-GT8 60mer glycan-masked mutants 15, 16, 21 and 33 have the preferred antigenic profiles

All 48 mutants were expressed in mammalian Expi293 cells using the same lumazine synthase nanoparticle format as the original eOD-GT8 60mer, and antigenic assessment was carried out directly on the cell supernatants. Two separate panels of antibodies were used: 1) CD4bs-specific antibodies to evaluate the antigenic integrity of the CD4bs and 2) non-CD4bs-specific antibodies to evaluate the extent of glycan-masking. The former panel included VRC01, its V gene germline revertant VRC01gl, and the VRC-PG04 V gene germline revertant VRC-PG04gl (Wu et al., 2011), whereas the latter panel included a polyclonal rabbit anti-gp120 serum, two non-CD4bs monoclonal antibodies (mAbs) (Figure 2A, X1A2 and X1C6) isolated from eOD-GT6 60mer-immunized XenoMouse (see STAR Methods), and two non-CD4bs mAbs (Figure 2A, mA9 and mE4) isolated from eOD-GT8 60mer-immunized IGHV1-2 knock-in mice (Tian et al., 2016). The non-CD4bs-specific antibodies and serum generally recognized eOD-GT8 and eOD-GT8 KO proteins equally well (Figures 2A and S1).

All but one (eOD-GT8-mut4 60mer) of the 13 single glycan mutants maintained strong binding to the CD4bs-specific antibodies, but none displayed decreased binding to all the non-CD4bs antibodies (Figure 2A). Compared to single glycan mutants, four multi-glycan mutants (eOD8-GT8-mut15, 16, 21 and 33 60mer) displayed preferable antigenic profiles (Figure 2A, marked by colored asterisks). Each showed strong recognition by CD4bs-specific mAbs and low binding to all or most non-CD4bs antibodies. Not surprisingly, these four mutants contained glycans which exhibited reduced recognition by non-CD4bs antibodies among the single glycan mutants (eOD8-GT8-mut1, 2, 4, 7 and 11 60mer) as well as glycans located on potentially immunogenic protruding loops (from eOD8-GT8-mut7, 10 and 11 60mer) (Figure 1D).

We purified the four best glycan-masked mutants for further characterization using affinity and size exclusion chromatography (Figure S2). These mutants were observed by ELISA to maintain high affinity to a panel of 11 VRC01-class germline revertant antibodies and four mature VRC01-class bNAbs, similar to the parental eOD-GT8 60mer (Figure 2B, left box). We also investigated the binding affinities of these glycan-masking mutants to a panel of 25 human VRC01-class antibody precursors (HuGL1-25) isolated from naive human B cells using an eOD-GT8 monomer as a probe (Jardine et al., 2016a). By ELISA, the four glycan mutants were observed to maintain strong binding to the high affinity precursors (Figure 2B, marked with black arrowheads) and to have reduced binding to lower affinity precursors relative to the parental eOD-GT8 60mer. When binding of 19 of these HuGL antibodies was examined by surface plasmon resonance (SPR), the antigen binding fragments (Fabs) of these precursors were observed to have affinities to eOD-GT8 ranging from 0.07 to 16 μM, consistent with the K_D values previously reported (Jardine et al., 2016a). The glycan mutants all showed less than a 4-fold reduction of binding affinity to these precursors relative to eOD-GT8 60mer (Figures 2C and 2D). eOD-GT8-mut16 60mer showed the least reduction (1.3-fold), with a geometric mean binding affinity of 2.5 μM to these human VRC01-class precursors compared to 2.0 μM for eOD-GT8 60mer. In summary, out of 48 mutants, eOD-GT8-mut15, 16, 21 and 33 60mer showed the best antigenic profiles for masking non-

CD4bs epitopes with minimal reduction in affinity to human VRC01-class bNAbs or their precursors.

Glycan-masked eOD-GT8 mutants 15, 16, 21 and 33 60mers contained introduced glycans and formed complete particles

We assessed the molecular assembly of the four best mutants (eOD-GT8-mut15, 16, 21 and 33) by negative stain EM. All four mutants formed spherical nanoparticles, similar to the parental eOD-GT8 60mer, with a lumazine synthase inner core of 16-18 nm in diameter and an eOD outer layer of 4.2-5.8 nm in thickness (Figure. 3A). We also examined the glycan occupancy at each predicted *N*-linked glycan sequon for the four eOD-GT8 60mer mutants and the parental eOD-GT8 60mer by liquid chromatography mass spectrometry (LC-MS). All ten predicted native *N*-linked glycosylation sites in the parental eOD-GT8 60mer had greater than 80% glycan occupancy (Figure 3B, green bars). For eOD-GT8-mut15, 16, 21 and 33 60mer, all added glycosylation sites had occupancies greater than 85% except the added N380 glycan (from single glycan mutant eOD-GT8-mut7) in eOD-GT8-mut16 and 21 60mer, which showed 59% and 73% occupancies respectively (Figure 3B, orange bars). In conclusion, eOD-GT8-mut15, 16, 21 and 33 60mer, each of which shared preferred antigenic binding profiles, also formed well assembled particles and were glycosylated at expected locations.

Glycan-masking of eOD-GT8 60mers focused the antibody response to the CD4bs in human IGHV1-2*02 knock-in mice

To investigate the impact of glycan-masking on focusing the antibody response to the CD4bs and the elicitation of VRC01-class precursors, we used a previously described homozygous IGHV1-2*02 knock-in mouse model (Tian et al., 2016). In this model, approximately 45% of naive B-cells express a human IGHV1-2*02 gene segment which in a given B cell is recombined with one of the 13 mouse D segments and one of the 4 mouse J_H segments to form diverse CDRH3s, and these heavy chains then pair with any one of the full repertoire of mouse light chains (Tian et al., 2016). To confirm the consistency and stability of the genotype of these transgenic mice, we bred and genotyped the mice and confirmed the persistence of the knock-in IGHV1-2*02 gene segment (Figure S3A). Based on fluorescence-activated cell sorting (FACS) analysis of several cell surface markers, splenic T and B cells, IgM^+ and IgG^+ B cell populations of IGHV1-2*02 knock-in mice appeared comparable to C57BL/6 and wildtype littermates (Figures S3B and S3C).

The immunogenicity of our most promising glycan-masked immunogens (eOD-GT8-mut15, 16, 21 and 33 60mer) was compared to the eOD-GT8 60mer control by immunizing these mice once using poly I:C as an adjuvant (Figure 4A). Two to three weeks after immunization, mice were sacrificed, serum and spleen collected, and the CD4bs-specific immune response in the serum or in the IgG^+ B cell compartment was analyzed using the eOD-GT8 monomer and its CD4bs-KO mutant, eOD-GT8 KO, as protein probes. As shown previously (Tian et al., 2016), the sera from eOD-GT8 60mer-immunized mice displayed similar reactivity to eOD-GT8 and eOD-GT8 KO, suggesting that much of the elicited serum response targeted non-CD4bs epitopes on eOD-GT8. By comparison, sera from mice immunized with the eOD-GT8 60mer glycan-masked mutants showed greater reactivity to

eOD-GT8 relative to the CD4bs KO mutant (Figure 4B). Quantification of this difference revealed that the percentage of the CD4bs-specific response increased from 42% in the eOD-GT8 60mer-immunized mice to 93%, 87%, 94% and 74% in the eOD-GT8-mut15, 16, 21 and 33 60mer-immunized mice, respectively (Figure 4C). Furthermore, the absolute CD4bs-specific serum response, as judged by the serum dilution (ED_{50}) difference in binding to eOD-GT8 versus eOD-GT8 KO, from the eOD-GT8-mut15, 16, and 33 60mer-immunized mice was higher than that from the eOD-GT8 60mer-immunized mice (2956, 7928, 4611 versus 2525, respectively); only eOD-GT8-mut21 60mer-immunized mice showed a decreased CD4bs-specific ED_{50} value (Figure 4C). These results indicated that the added glycans in eOD-GT8-mut15, 16 and 33 60mer resulted in a substantially reduced serum response to non-CD4bs epitopes while maintaining accessibility to the CD4bs.

We also determined the frequency of CD4bs-specific B cells among eOD-GT8-specific IgG^+ B cells ($B220^+IgG^+$) by using fluorophore-labeled eOD-GT8 and eOD-GT8 KO monomers as probes (Jardine et al., 2015; Sok et al., 2016; Tian et al., 2016). CD4bs-specific B cells were defined as those that bound to eOD-GT8 but not to the CD4bs-KO version of eOD-GT8, whereas the non-CD4bs-specific B cells corresponded to those that bound to both eOD-GT8 and eOD-GT8 KO (Figure 4D). The frequency of the CD4bs-specific B cells in the total IgG^+ B cell population was increased from a mean of 1.1% in the eOD-GT8 60mer-immunized group to 4.2%, 2.7% and 3.3% in the eOD-GT8-mut15, 16 and 33 60mer-immunized groups, respectively. Likewise, average non-CD4bs-specific B cell frequency in the total IgG^+ B cell population was reduced from 2.5% in the eOD-GT8 60mer-immunized group to 0.7%, 1.2% and 1.0% in the eOD-GT8-mut15, 16 and 33 60mer-immunized groups (Figure 4E). eOD-GT8-mut21 60mer was an exception in that it elicited a reduced frequency of both CD4bs-specific and non-CD4bs IgG^+ B cells. The frequency of the CD4bs-specific IgG^+ B cells among all elicited $eOD\text{-}GT8^+$ IgG^+ B cells increased from a mean of 37% in the eOD-GT8 60mer-immunized control group to 87%, 73%, 77% and 83% in eOD-GT8-mut15, 16, 21 and 33 60mer-immunized groups, respectively (Figure 4F). To address the possibility that the mice may have mounted an immune response against neo-epitopes generated by glycan masking that parental eOD-GT8-based probes would not detect, we also examined sera and B cell responses from the respective immunization groups using immunogen-matched eOD-GT8-mut15, 16 and 33 probes. Since ELISA and flow cytometry assays indicated similar CD4bs-specific serum and B cell responses between the probe sets (Figure S4), we continued to use eOD-GT8 and eOD-GT8 KO probes for the rest of the study.

To evaluate the effect of different immunogen doses and types of adjuvants as well as an additional boost on the elicitation of VRC01-class antibodies, we performed two further experiments using the same mouse model (Figures 5 and S3E). Similar increases in frequency of both the CD4bs-specific serum response and the CD4bs-specific IgG^+ B cell response were consistently observed for eOD-GT8-mut15, 16 and 21 60mer, relative to eOD-GT8 60mer, when immunizations were performed with different dosages or different adjuvants (Figures 5A-C). Evaluation of two additional mutants, eOD-GT8-mut17 and 18, in an independent immunization study at a 30 μg dose, also revealed comparable results (Figure 5B and 5C). Finally, when we analyzed the results from all immunization experiments together, we observed statistically higher CD4bs-specific serum responses for

immunogens eOD-GT8-mut15 60mer and eOD-GT8-mut16 60mer relative to eOD-GT8 60mer (Figure 6A) and statistically higher frequencies of CD4bs-specific B cells were observed for all six evaluated immunogens relative to eOD-GT8 60mer (Figure 6B).

In summary, glycan-masking of the eOD-GT8 60mer immunogen was shown to increase the elicitation of CD4bs-specific serum antibodies in both overall titers (Figures 4C) and as a percentage of antigen-specific response (Figures 4C, 5B, and 6A). Moreover, glycan-masking of eOD-GT8 increased the CD4bs-specific IgG^+ B cell frequency among both eOD-GT8-specific IgG^+ B cells (Figure 4F, 5C, and 6B) and total IgG^+ B cells (Figures 4E).

Glycan-masking of eOD-GT8 60mers enhanced the elicitation of VRC01-class antibodies in human IGHV1-2*02 knock-in mice

To determine whether glycan-masked eOD-GT8 60mer immunogens elicited VRC01-class precursors in IGHV1-2*02 knock-in mice, we performed single cell RT-PCR on splenic antigen-sorted CD4bs-specific IgG^+ B cells from these immunized mice as described previously (Tian et al., 2016). In most cases, we first amplified and sequenced the Igκ light chains of the IgG antibodies expressed by the sorted B cells to search for a 5-amino acid CDRL3, a signature of VRC01-class antibodies. From B cells that exhibited this Igκ light chain signature, we then amplified and sequenced their corresponding heavy chains to confirm that the light chains were paired with human IGHV1-2 heavy chains. Consistently, all 5-amino acid CDRL3 Igκ light chains, for which we could amplify a paired heavy chain, were found to pair with the human IGHV1-2. Thus, we could use the number of CD4bs-specific B-cells expressing a 5-amino acid CDRL3 Igκ light chain as a measure of the number of VRC01-class precursor antibodies (Sok et al., 2016). We subsequently calculated the frequency of VRC01-class precursors (containing a human IGHV1-2 heavy chain and a mouse light chain with 5-amino acid CDRL3) across all three immunization studies relative to the total number of sequenced Igκ light chains within each respective immunogen group. This frequency was calculated per mouse (Figure 6C and Tables S2-S4), as a mean value for immunized animals (Figure 6C) and as an overall frequency per immunogen (Figures 6D). By this analysis, we observed an average of 3.2% of the amplified Igκ light chains from CD4bs specific B cells elicited from eOD-GT8 60mer immunization had the VRC01-class antibody signature. In contrast, the mean value of VRC01-class precursors from mice immunized with eOD-GT8-mut15, 16 or 33 60mer was 7.0%, 9.1%, and 3.7%, respectively (Figures 6C). Notably, eOD-GT8-mut16 60mer elicited a statistically significant (Mann-Whitney test, p=0.007) 2.8-fold increase in the mean frequency of VRC01-class antibodies relative to eOD-GT8 60mer (9.1% vs 3.2%) (Figure 6C, ANOVA Kruskal-Wallis test, p=0.0159) and a 4.2-fold increase in the overall frequency of VRC01-class antibodies among the cloned CD4bs-specific antibodies (9.7% vs 2.3%) (Figure 6D).

The CDRL3s of the isolated VRC01-class antibody precursors elicited by eOD-GT8-mut15, 16, 17 and 21 60mer were found to be enriched for the QQY motif found in the VRC01 antibody. CDRL3 sequences elicited by the eOD-GT8-mut16 60mer showed some enrichment for Q at position 96 (observed in 11 out of 28 sequences), but the other immunogens did not enrich for the E/Q residue found in mature VRC01-class antibodies (Figure 6E). Based on the observed Igκ V- and J-gene usage and CDRL3 sequences, five

VRC01-class antibody light chain lineages were shared between antibodies elicited by parental eOD-GT8 60mer and glycan-masked eOD-GT8 60mer mutants, suggesting that the same sets of light chain unmutated common ancestors (UCAs) were stimulated by these immunogens (Table S5, boxed in black). The CDRH3s of the cloned VRC01-class precursors varied in sequence and length, ranging from 7-15 amino acids, consistent with the diverse CDRH3s associated with IGHV1-2*02 in this mouse model and in human PBMCs (Jardine et al., 2016a; Tian et al., 2016). Since these mice were immunized only once or twice, heavy chains of the isolated VRC01-class precursors accumulated minimal SHM (<6.5%) (Figure S5 and Table S6). In summary, these data showed that glycan-masking of eOD-GT8 enhanced the elicitation of VRC01-class precursors in the immunized IGHV1-2*02 knock-in mice.

Discussion

The eOD-GT8 60mer has been shown to elicit VRC01-class precursors in IGHV1-2*02 knock-in mouse models (Dosenovic et al., 2015; Jardine et al., 2015). In the mouse model used here, IGHV1-2*02 recombines with the normal complement of mouse D_H and J_H gene segments, thereby allowing the generation of B cells that express a diverse array of CDRH3s in the IGHV1-2*02 heavy chain. Another feature of this mouse model is that IGHV1-2*02 is located at the most proximal end of the mouse V_H cluster relative to D segments. The proximity, along with the deletion of the IGCR1 regulatory element in the V_H-D intervening region, strongly favors the utilization of IGHV1-2*02 during V(D)J recombination (Tian et al., 2016). For this reason, IGHV 1-2*02 heavy chains account for 45% of total heavy chains (Tian et al., 2016), a frequency which is 15.5 times higher than that in naive B cells of human PBMCs (2.9 ± 1.3 %) (Sok el al, 2016). Five-amino acid CDRL3 Igκ chains were detected at a frequency of 0.15% (Tian et al., 2016), which is 6.3 times lower than the frequency in human PBMCs (0.95 ± 0.57%) immunized IGHV1-2*02 knock-in mice. (Sok el al, 2016). Overall, we estimated that the potential VRC01-class precursors were expressed in this mouse model at a frequency of 0.068% (45% × 0.15%), which is approximately 2.4-fold higher than in humans (2.9% × 0.95%). The higher frequency of potential VRC01-class precursors helped to compensate for the small size of the B cell compartment in mice. Thus, in terms of absolute number and diversity of B cells expressing potential VRC01 precursors, the IGHV1-2*02-rearranging mouse model may offer a closer approximation to the human repertoire than conventional knock-in mice. eOD-GT6 (Jardine et al., 2013), a VRC01-class immunogen with lower affinity than eOD-GT8, which failed to isolate VRC01-class naive B cells from human PBMCs (Jardine et al., 2016a), also failed to elicit VRC01-class precursors at detectable level in this mouse model, highlighting the stringency of the model. In a prior study, we were able to elicit VRC01-class antibodies with a single immunization of eOD-GT8 60mer, though many of the elicited antibodies and IgG^+ B cells targeted non-CD4bs epitopes (Tian et al., 2016).

To more effectively focus the antibody immune response to the CD4bs, we used sequence and structural information to selectively add *N*-linked glycans to mask the non-CD4bs regions of eOD-GT8. In three independent experiments with different adjuvants and immunization schema in the IGHV1-2-rearranging mouse model, glycan-masking mutants were shown to enhance the specificity of CD4bs responses in both sera and the IgG^+ B cell

pools with the best results observed for the eOD-GT8-mut16 60mer. Moreover, VRC01-class precursor B cell receptors (BCRs) were isolated at higher frequencies from mice immunized with glycan-masking mutants than those immunized with eOD-GT8 60mer, with the highest frequency in eOD-GT8-mut16 60mer-immunized mice. By blocking non-CD4bs epitopes, which are often dominant and more immunogenic than the CD4bs epitope, we likely reduced the competition that the VRC01-class B cell precursors would face during their activation and maturation, and provided a greater opportunity to access limited resources such as antigen-presenting cells and T cell help and to mature into IgG-secreting B cells. As noted earlier, this mouse model over represented the number of VRC01-class precursor B-cells, compared to the naive human repertoire. Thus, it is difficult to predict how much improvement might be attained with a glycan variant compared to the wild type eOD-GT8 in humans. A phase I study of the eOD-GT8 60mer is planned to begin later this year. If this immunogen is shown to elicit VRC01 class antibodies in humans, it is reasonable to expect that improved variants, such as those described here, could further focus the immune response on the CD4bs.

Of note, glycans not crowded by other glycans can have a degree of conformational flexibility that enlarges their footprint on the protein surface (Stewart-Jones et al., 2016). Thus, the added glycans, especially those near the CD4bs, such as glycans at residue 268, 380 and 482, may have restricted the approach angles from which a CD4bs-specific BCR could access the CD4bs. Accordingly, only those BCRs with an optimal approach angle would have had the potential to develop into VRC01-class bnAbs. Among the 25 potential VRC01-class precursors isolated from naive human B cells, the top nine antibodies with the highest eOD-GT8 binding affinities (K_D < 3μM) recognized all of the glycan mutants with affinities comparable to their interaction with eOD-GT8 60mer. However, the lower affinity human precursor antibodies bound the glycan mutants much more weakly than to eOD-GT8 60mer. These lower affinities may have been due to approach angles not optimally compatible with added glycans, although eOD-GT8 interactions with germline-encoded VH1-2 should significantly constrain the angle of approach. The glycan mutants may have therefore preferentially selected for high affinity precursors, which may have included those with optimal approach angles, but may have also reduced capacity to prime lower affinity precursors. A recent study has shown that antibody precursor affinity towards its cognate immunogen can have a large effect on B cell recruitment, differentiation and antibody maturation (Abbott et al., 2017). Thus, the ability of glycan mutants to further focus the antibody response while maintaining high affinity to target antibody precursors is a potential improvement in germline targeting vaccine design.

The initial ELISA analysis of 13 individual mutants indicated that eOD-GT8-mut1, 2, 4, 5, 7, 11 and 23 60mer were among the best at masking the binding of non-CD4bs antibodies. Five of these glycans (from eOD-GT8-mut1, 2, 4, 5 and 23) are all clustered together in the same region (cluster 1) on a face opposite the CD4bs (Figure S6B), suggesting that this may be an immunogenic hotspot. The other two glycans, from eOD-GT8-mut7 and 11, are both located on nearby protruding loops which may represent another immunogenic hotspot (cluster 2). Only two of these seven glycans, from eOD-GT8-mut1 and 2, would be accessible in the context of the envelope trimer. The rest of the glycans mask new surfaces created in the context of an isolated eOD and thus served to block undesired neoepitopes in

this immunogen. Of the four best glycan combination mutants examined (eOD-GT8-mut15, 16, 21 and 33), each had at least two glycans from the first cluster and one or more glycans from the second cluster, suggesting that both glycan clusters may have been important for suppressing elicitation of non-CD4bs antibodies. Notably, eOD-GT8-mut15 60mer, which had only three added glycans, performed very well in immune focusing relative to the other three mutants with 4-6 added glycans. This suggested that the three glycans in eOD-GT8-mut15 sufficed to cover the most dominant off-target surfaces. However, eOD-GT8-mut16 60mer with five added glycans was ultimately the most specific for the elicitation of CD4bs-specific serum and of VRC01-class precursors, which may have been due, in part, to the fact that this mutant retained affinities nearly as high as eOD-GT8 for human naive VRC01-class precursors. Although shown to be an effective prime, the glycan-masked versions of eOD-GT8 60mer would likely require further vaccine boosts with immunogens designed to direct affinity maturation of the initial antibody recombinants to resemble mature VRC01-class bNAbs. This will likely entail design of intermediate immunogens that more closely resemble prevalent strains at the CD4bs epitope (Briney et al., 2016; Steichen et al., 2016; Escolano et al., 2016; Tian et al., 2016).

In summary, we used structure-guided glycan-masking, followed by antigenic characterization, to identify variants of the eOD-GT8 60mer immunogen capable of focusing the immune response on the CD4bs and, specifically, to improve the ability of this germline-targeting priming immunogen to elicit VRC01-class responses, an important class of HIV-1 neutralizing antibodies. The enhanced antibody response elicited by these glycan-masked immunogens may facilitate the ability of subsequent boost immunizations to maturate these antibody precursors into HIV-1 neutralizing antibodies. The best of these glycan mutants, eOD-GT8-mut16 60mer, may serve as a second generation of eOD-GT8 60mer for further evaluation in clinical trials. Our results suggested that glycan-masking could be applied to focus immune responses to key epitopes on other HIV-1 immunogens or vaccine candidates for other pathogens.

STAR*Methods

CONTACT FOR REAGENT AND RESOURCE SHARING

Further information and requests for resources and reagents should be directed to and will be fulfilled by the Lead Contact, John R. Mascola (jmascola@nih.gov).

EXPERIMENTAL MODEL AND SUBJECT DETAILS

Generation and characterization of IGHV1-2 single knock-in mouse models— The generation and characterization of the IGHV1-2*02 mouse model used in this study have been described in detail in a previous publication (Tian et al., 2016). Briefly, human IGHV1-2*02 segment substitutes for the mouse V_H81X segment at the IgH locus, and IGCRI was deleted from the same IgH allele. In this setting, IGHV1-2*02 segment is preferentially utilized for V(D)J recombination and accounts for about 45% of heavy chains in the antibody repertoire. These genetic modifications were introduced into EF1 ES cell line, which was derived from an F1 hybrid mouse (129/Sv and C57BL/6). IGHV1-2*02 replacement and IGCRI deletion occurred on the IgH allele from the 129/Sv strain.

Correctly modified ES clones were injected into Rag2 deficient blastocysts to generate chimeric mice (Chen et al. 1993). The chimeric mice were bred with the 129/Sv strain mice for germline transmission. Heterozygous IGHV1-2*02 knock-in mice were interbred to produce homozygous knock-in mice, which are used for the experiments in this study. Ten to 14-week-old female/male homozygous IGHV1-2*02 mice were used for all the experiments. Littermates were randomly assigned to experimental groups for each independent study. All the mice were housed in the animal facility of the Vaccine Research Center (VRC), NIAID, NIH, Bethesda, MD. All animal experiments were reviewed and approved by the Animal Care and Use Committee of the Vaccine Research Center, NIAID, NIH, and all animals were housed and cared for in accordance with local, state, federal, and institute policies in an American Association for Accreditation of Laboratory Animal Care (AAALAC)-accredited facility at the NIH. For B cell characterization, splenic B cells were stained with anti-B220, anti-IgM, anti-IgD, anti-IgG antibodies and analyzed with flowcytometry.

Human: Expi293F™ cells—Expi293F™ cells were purchased from ThermoFisher Scientific Inc. (Invitrogen, cat# A14528; RRID: CVCL_D615) for protein production. It is derived from the HEK293-F cell line, originating from a female fetus.

Method Details

Design of eOD-GT8 glycan-masking mutants.—Using the crystal structure of eOD-GT8 monomer (Jardine et al., 2016a), we identified all surface residues with exposed Cβ atoms (or Cα in the case of glycine) equal to or greater than 5Å from the CD4bs and from potential native glycans and these were designated as non-CD4bs residues. Each non-CD4bs position was examined using PyMol (The PyMol Molecular Graphics System, version 1.8.6; Schrödinger, LLC) for the potential structural effects of incorporating an NxT sequon (where X is not a proline). NxT sequons were used instead of NxS since they are known to glycosylate more efficiently than NxS sequons (Kaplan et al., 1987; Kasturi et al., 1995). Positions where the introduction of asparagine or the downstream *i*+2 threonine could potentially decrease protein stability (e.g. by steric clash, loss of hydrogen bond, interruption of hydrophobic core packing, etc.) were discarded. The remaining positions were further evaluated for sequence-based glycosylation potential using the NetNGlyc server (http://www.cbs.dtu.dk/services/NetNGlyc/). Glycosylation sites with scores less than 0.5 were discarded. Each potential glycan was also modeled onto the eOD-GT8 structure using the program Glycosylate (He and Zhu, 2015) to aid in the visual inspection of potential glycan locations as well as the selection of various glycans to combine together in individual designs. The identification of new glycan sites located on protruding loops was performed by examining the monomer eOD-GT8 crystal structure using Pymol. For one sequon (at Hxbc2 residue 268), the preceding glutamate was mutated to glycine to further reduce the immunogenicity of this site (Hopp and Woods, 1981). For another sequon (at Hxbc2 residue 419) a glycine was introduced just after the sequon to counter the low glycosylation potential caused by the adjoining proline (Mellquist et al., 1998). For five of the mutants (eOD-GT8-mut22, 23, 40, 41 and 45), an additional set of two residues were also mutated to reduce immunogenicity (E267G and E268G) or to improve overall stability (I477L and D478N). See Table S1. All structural figures were created using the eOD-GT8 crystal

structure (PDB 5IES) as a template and the molecular graphics program PyMol (The PyMol Molecular Graphics System, version 1.8.6; Schrödinger, LLC).

Immunizations—100 μl of immunogen mix, containing 30-60 μg of specified protein immunogen and 60 μg of poly I:C (InvivoGen, high molecular weight) or 50ul of Sigma Adjuvant System reconstituted with 1ml of PBS per vial (Sigma) in PBS, was injected to the inner thigh of the two rear legs of each mouse. IGHV1-2 mice were immunized once or twice with 4 weeks interval, and blood and spleens were collected two weeks after the last immunization.

Isolation of non-CD4bs monoclonal antibodies—Transgenic XenoMouse™ that expresses human immunoglobulins (Jakobovits et al., 2007) were immunized twice with 15 μg of eOD-GT6 60mer (Jardine et al., 2013a) plus 30 μg of poly I:C with a one week interval. The mice were sacrificed two weeks after the last injection. Splenocytes were used to sort for B cells stained positively for both eOD-GT6 and eOD-GT6 CD4bs-KO mutant antigen probes. Human IgG heavy and light chains were cloned from these cells as described previously (Wu et al., 2010) and expressed in pairs in Expi293 cells. Two purified XenoMouse IgGs, X1A2 and X1C6, were confirmed to be non-CD4bs-specific and eOD-GT8 reactive by ELISA and bound equally well to both eOD-GT8 and the eOD-GT8 CD4bs KO mutant (Figure 2A and S1). Similarly, two non-CD4bs IgGs, mA9 and mE4, were cloned from IGHV1-2*02 single knock-in mice that had been immunized once with 60 μg of eOD-GT8 60mer plus 60 μg of poly I:C (Tian et al., 2016). These two antibodies use human IGHV1-2*02 paired with mouse kappa chains and both bound to eOD-GT8 and eOD-GT8 KO equally well (Figure 2A).

Protein production—All proteins were produced in transiently transfected Expi293 cells as previously described (Cheng et al., 2015; Pancera et al., 2014). Briefly, cell supernatants were collected 6-7 days after transfection, filtered and concentrated as needed. The immunogens, eOD-GT8_60mer (lumazine synthase nanoparticle) and its glycan mutants were purified with *Galanthus nivalis* (GNA)-lectin gel (EY Laboratories, Inc.) followed by gel filtration chromatography. ELISA and sorting probes, avi-his-tagged eOD-GT8 and its CD4bs-KO mutant, eOD-GT8 KO (D279K/D368R), were purified with Ni-NTA beads (GE healthcare) followed by gel filtration chromatography for isolation of monomeric protein. Antibodies were purified with protein A or G sepharose 4B (GE healthcare).

Negative-stain electron microscopy.—Samples were diluted to ~0.05 mg/ml, adsorbed to freshly glow-discharged carbon-film grids for 15 s, and stained with 0.75% uranyl format. For 2D analysis, images were collected semi-automatically using SerialEM (Mastronarde, 2005) on an FEI Tecnai T20 electron microscope equipped with a 2k × 2k Eagle CCD camera. Reference-free 2D classification was performed using EMAN2.1 (Tang et al., 2007).

ELISA

ELISAs were performed as previously described (Tian et al., 2016). One exception was for initial screening of eOD-GT8 60mer glycan mutants expressed in Expi293 cell supernatants.

For this process, we first coated Costar half area plates with 50 μl /well of 1μg/ml *Galanthus Nivalis* lectin (Sigma) in PBS at 4°C overnight, blocked the wells with 1:10 diluted blocking solution (Immune Technology Corp.), and then applied excess amount (based on yield of eOD-GT8 60mer in Expi293 and confirmed experimentally) of the cell supernatants containing expressed eOD-GT8 60mer or its glycan mutants to fully load the bound lectin and ensure equal loading of eOD-GT8 60mer or mutant nanoparticles in each well. Later steps of ELISA were the same as described previously (Tian et al., 2016). Briefly, both primary and secondary antibody incubation were performed at room temperature for 1 hour. Plates were washed 5x with PBS/T after each incubation step, 1:5,000 diluted HRP-conjugated goat-anti-mouse or goat-anti-human IgGs (Bio-Rad) were used as secondary antibody, and SuperBlue™ TMB Microwell peroxidase substrate (Kirkegaard & Perry Laboratories, Inc.) was used for color development that was terminated with 1N H_2SO_4. OD450 was read with a SpectraMax Plus384 plate reader (Molecular Devices, LLC.). ELISA data were quantified by calculating the ED_{50} (dilution factor) of total antigen-specific (based on eOD-GT8 binding curves), non-CD4bs-specific (based on eOD-GT8 KO binding curves) and CD4bs-specific ("total" minus "non-CD4bs") responses, and by calculating the ED_{50}-based percentages of non-CD4bs-specific and CD4bs-specific responses in the total antigen-specific sera.

Flow cytometry and single B-cell sorting—Mouse spleen samples were processed for single B cell sorting based on previously described methods (Tian, et al, 2016). Briefly, single cell suspension of splenocytes was stained sequentially with ViViD and a staining mix containing anti-CD3 PerCP-Cy5.5, anti-CD4 PerCP-Cy5.5, anti-CD8 PerCP-Cy5.5, anti-F4/80 PerCP-Cy5.5, anti-B220 PE-TR, anti-IgD BV711, anti-IgM PE-Cy7, anti-IgG (1, 2a, 2b, and 3) FITC, eOD-GT8-PE and eOD-GT8 KO-APC. IgG+ B cells with eOD-GT8-PE+ eOD-GT8 KO-APC-were selected and single-cell sorted into 96 well plates containing lysis buffer on a BD FACSAria III sorter and immediately stored at −80°C. FlowJo Ver.9.9.3 software was used to analyze the Flow cytometry data.

Single B-cell RT-PCR, gene amplification, cloning and mutation analysis of cloned IgH and IgL chains—Reverse transcription and subsequent PCR amplification of heavy and light chain variable genes were performed using SuperScript III (Life Technologies) as previously described (Tiller et al., 2009; Wu et al., 2010). Briefly, mixtures of mouse Ig primers (Tiller et al., 2009) were supplemented with human VH1-2 specific primers for 1st and 2nd PCR (Tian, et al, 2016). PCR products were then sequenced using Sanger sequencing and corrected for PCR errors before further analysis. Frequencies of VRC01-class antibodies among amplified Igκ light chains were calculated by dividing the total numbers of isolated VRC01-class antibodies in each mouse with total numbers of amplified Igκ light chains in each mouse. Sequence logo images were created by the WebLogo server (http://weblogo.berkeley.edu/logo.cgi) (Crooks et al., 2004). CDRL3 sequences of eOD-GT8 60mer-elicited antibodies are from 7 antibodies in this study and 17 antibodies from previous published study in the same VH1-2*02 KI mice immunized with eOD-GT8 60mer at 30 or 60 μg once with Poly I:C adjuvant (Tian et al., 2016).

Surface plasmon resonance (SPR)—Affinities of antibody-antigen interactions were measured as previously described (Jardine et al., 2015; Tian et al., 2016). Briefly, we measured kinetics and affinities of antibody-antigen interactions on a ProteOn XPR36 (Bio-Rad) using GLC Sensor Chip (Bio-Rad) and 1x HBS-EP+ pH 7.4 running buffer (20x stock from Teknova, Cat. No H8022) supplemented with BSA at 1mg/ml. We followed the Human Antibody Capture Kit instructions (Cat. No BR-1008-39 from GE) to prepare chip surfaces for ligand capture. In a typical experiment, about 6000 RU of capture antibody was amine-coupled in all 6 flow cells of the GLC Chip. Regeneration was accomplished using 3M Magnesium Chloride with 180 seconds contact time and injected four times per each cycle. Raw sensorgrams were analyzed using ProteOn Manager software (Bio-Rad), including interspot and column double referencing, and either Equilibrium fits or Kinetic fits with Langmuir model, or both, were employed when applicable. Analyte concentrations were measured on a NanoDrop 2000c Spectrophotometer using Absorption signal at 280 nm.

Mass Spectrometry Glycan Analysis—An aliquot of each sample was denatured by incubating with 10 mM of dithiothreitol at 56 °C for an hour and alkylated by 55 mM of iodoacetamide for 45 minutes in dark prior to digestion with proteases optimized based on amino acid sequence of each target protein. Specifically, each aliquot was treated with Arg-C (Promega) and Glu-C (Promega) sequentially. Following digestion, the samples were deglycosylated by Endo-H (Promega) followed by PNGaseF (Glyko®, Prozyme) treatment in the presence of O18-water. The resulting peptides were separated on an Acclaim PepMap RSLC C18 column (75 μm × 15 cm) and eluted into the nano-electrospray ion source of an Orbitrap Fusion™ Lumos™ Tribrid™ mass spectrometer (Thermo Fisher Scientific) with a 180-min linear gradient consisting of 0.5-100% solvent B over 150 min at a flow rate of 200 nL/min. The spray voltage was set to 2.2 kV and the temperature of the heated capillary was set to 280 °C. Full MS scans were acquired from m/z 300 to 2000 at 60k resolution, and MS2 scans following collision-induced fragmentation were collected in the ion trap for the most intense ions in the Top-Speed mode within a 5-sec cycle using Fusion instrument software (v2.0, Thermo Fisher Scientific). The resulting spectra were analyzed using SEQUEST (Proteome Discoverer 1.4, Thermo Fisher Scientific) with full MS peptide tolerance of 20 ppm and MS2 peptide fragment tolerance of 0.5 Da, and filtered using ProteoIQ (v2.7, Premier Biosoft) at the protein level to generate a 1% false discovery rate for protein assignments. Site occupancy was calculated using spectral counts assigned to the O18-Asp-containing (PNGaseF-cleaved) and/or HexNAc-modified (EndoH-cleaved) peptides and their unmodified counterparts.

Quantification and statistical analysis—Statistical comparisons using GraphPad Prism 7.01 Software (GraphPad Prism Software, Inc.) were performed only on the combined data sets with n>3. For these comparisons overall nonparametric ANOVA Kruskal-Wallis tests were performed and if the *p*-values were less than 0.05 they were followed by nonparametric Mann-Whitney tests between two individual groups.

DATA AND SOFTWARE AVAILABILITY

The sequences of 73 elicited VRC01-class antibodies reported in this paper have been deposited at GenBank: MH485280 - MH485352 for the heavy chains and MH485207 - MH485279 for the light chains.

Supplementary Material

Refer to Web version on PubMed Central for supplementary material.

Acknowledgements

We thank Richard Nguyen and Ambrozak David for assistance in single-cell sorting, Marlon Dillon and Salbador Gloria for animal care and maintenance, Sam Darko for assistance with data analysis and members of the Structural Biology Section of the Vaccine Research Center for helpful discussions. This work was supported by the intramural research program of the Vaccine Research Center, NIAID, NIH. Support for this work was also provided by federal funds from the Frederick National Laboratory for Cancer Research, National Institutes of Health, under contract HHSN261200800001E, and Leidos Biomedical Research, Inc. (T.S., Y.T.). The work was also supported by NIAID UM1AI100663 (CHAVI-ID) (W.R.S.) and the International AIDS Vaccine Initiative Neutralizing Antibody Consortium and Center with support from the United States Agency for International Development, the Ministry of Foreign Affairs of the Netherlands, and the Bill & Melinda Gates Foundation; a full list of IAVI donors is available at www.iavi.org (W.R.S.).

References

Abbott RK, Lee JH, Menis S, Skog P, Rossi M, Ota T, Kulp DW, Bhullar D, Kalyuzhniy O, Havenar-Daughton C, et al. (2017). Precursor Frequency and Affinity Determine B Cell Competitive Fitness in Germinal Centers, Tested with Germline-Targeting HIV Vaccine Immunogens. Immunity 48, 133–146. [PubMed: 29287996]

Ahmed FK, Clark BE, Burton DR, and Pantophlet R (2012). An engineered mutant of HIV-1 gp120 formulated with adjuvant Quil A promotes elicitation of antibody responses overlapping the CD4-binding site. Vaccine 30, 922–930. [PubMed: 22142583]

Briney B, Sok D, Jardine JG, Kulp DW, Skog P, Menis S, Jacak R, Kalyuzhniy O, de Val N, Sesterhenn F, et al. (2016). Tailored Immunogens Direct Affinity Maturation toward HIV Neutralizing Antibodies. Cell 166, 1459–1470. [PubMed: 27610570]

Burton DR, and Hangartner L (2016). Broadly Neutralizing Antibodies to HIV and Their Role in Vaccine Design. Annu Rev Immunol 34, 635–659. [PubMed: 27168247]

Chen J, Lansford R, Stewart V, Young F, and Alt FW (1993). RAG-2-deficient blastocyst complementation: an assay of gene function in lymphocyte development. Proc Natl Acad Sci U S A 90, 4528–4532. [PubMed: 8506294]

Cheng C, Pancera M, Bossert A, Schmidt SD, Chen RE, Chen X, Druz A, Narpala S, Doria-Rose NA, McDermott AB, et al. (2015). Immunogenicity of a Prefusion HIV-1 Envelope Trimer in Complex with a Quaternary-Structure-Specific Antibody. J Virol 90, 2740–2755. [PubMed: 26719262]

Crooks GE, Hon G, Chandonia JM, and Brenner SE (2004). WebLogo: a sequence logo generator. Genome Res 14, 1188–1190. [PubMed: 15173120]

Dey B, Pancera M, Svehla K, Shu Y, Xiang SH, Vainshtein J, Li YX, Sodroski J, Kwong PD, Mascola JR, et al. (2007). Characterization of human immunodeficiency virus type 1 monomeric and trimeric gp120 glycoproteins stabilized in the CD4-bound state: Antigenicity, biophysics, and immunogenicity. Journal of Virology 81, 5579–5593. [PubMed: 17360741]

Dey B, Svehla K, Xu L, Wycuff D, Zhou TQ, Voss G, Phogat A, Chakrabarti BK, Li YX, Shaw G, et al. (2009). Structure-Based Stabilization of HIV-1 gp120 Enhances Humoral Immune Responses to the Induced Co-Receptor Binding Site. Plos Pathogens 5, e1000445. [PubMed: 19478876]

Dosenovic P, von Boehmer L, Escolano A, Jardine J, Freund NT, Gitlin AD, McGuire AT, Kulp DW, Oliveira T, Scharf L, et al. (2015). Immunization for HIV-1 Broadly Neutralizing Antibodies in Human Ig Knockin Mice. Cell 161, 1505–1515. [PubMed: 26091035]

Escolano A, Steichen JM, Dosenovic P, Kulp DW, Golijanin J, Sok D, Freund NT, Gitlin AD, Oliveira T, Araki T, et al. (2016). Sequential Immunization Elicits Broadly Neutralizing Anti-HIV-1 Antibodies in Ig Knockin Mice. Cell 166, 1445–1458. [PubMed: 27610569]

Forsell MNE, Soldemo M, Dosenovic P, Wyatt RT, Karlsson, and Hedestam GBK (2013). Independent Expansion of Epitope-Specific Plasma Cell Responses upon HIV-1 Envelope Glycoprotein Immunization. Journal of Immunology 191, 44–51.

Garrity RR, Rimmelzwaan G, Minassian A, Tsai WP, Lin G, de Jong JJ, Goudsmit J, and Nara PL (1997). Refocusing neutralizing antibody response by targeted dampening of an immunodominant epitope. J Immunol 159, 279–289. [PubMed: 9200464]

Gautam R, Nishimura Y, Pegu A, Nason MC, Klein F, Gazumyan A, Golijanin J, Buckler-White A, Sadjadpour R, Wang K, et al. (2016). A single injection of anti-HIV-1 antibodies protects against repeated SHIV challenges. Nature 533, 105–109. [PubMed: 27120156]

He L, and Zhu J (2015). Computational tools for epitope vaccine design and evaluation. Curr Opin Virol 11, 103–112. [PubMed: 25837467]

Hoot S, McGuire AT, Cohen KW, Strong RK, Hangartner L, Klein F, Diskin R, Scheid JF, Sather DN, Burton DR, et al. (2013). Recombinant HIV envelope proteins fail to engage germline versions of anti-CD4bs bNAbs. PLoS Pathog 9, e1003106. [PubMed: 23300456]

Hopp TP, and Woods KR (1981). Prediction of Protein Antigenic Determinants from Amino-Acid-Sequences. P Natl Acad Sci-Biol 78, 3824–3828.

Huang J, Kang BH, Ishida E, Zhou T, Griesman T, Sheng Z, Wu F, Doria-Rose NA, Zhang B, McKee K, et al. (2016). Identification of a CD4-Binding-Site Antibody to HIV that Evolved Near-Pan Neutralization Breadth. Immunity 45, 1108–1121. [PubMed: 27851912]

Ingale J, Tran K, Kong L, Dey B, McKee K, Schief W, Kwong PD, Mascola JR, and Wyatt RT (2014). Hyperglycosylated stable core immunogens designed to present the CD4 binding site are preferentially recognized by broadly neutralizing antibodies. J Virol 88, 14002–14016. [PubMed: 25253346]

Jakobovits A, Amado RG, Yang X, Roskos L, and Schwab G (2007). From XenoMouse technology to panitumumab, the first fully human antibody product from transgenic mice. Nat Biotechnol 25, 1134–1143. [PubMed: 17921999]

Jardine J, Julien JP, Menis S, Ota T, Kalyuzhniy O, McGuire A, Sok D, Huang PS, Macpherson S, Jones M, et al. (2013). Rational HIV Immunogen Design to Target Specific Germline B Cell Receptors. Science 340, 711–716. [PubMed: 23539181]

Jardine JG, Kulp DW, Havenar-Daughton C, Sarkar A, Briney B, Sok D, Sesterhenn F, Ereno-Orbea J, Kalyuzhniy O, Deresa I, et al. (2016a). HIV-1 broadly neutralizing antibody precursor B cells revealed by germline-targeting immunogen. Science 351, 1458–1463. [PubMed: 27013733]

Jardine JG, Ota T, Sok D, Pauthner M, Kulp DW, Kalyuzhniy O, Skog PD, Thinnes TC, Bhullar D, Briney B, et al. (2015). Priming a broadly neutralizing antibody response to HIV-1 using a germline-targeting immunogen. Science 349, 156–161. [PubMed: 26089355]

Jardine JG, Sok D, Julien JP, Briney B, Sarkar A, Liang CH, Scherer EA, Henry Dunand CJ, Adachi Y, Diwanji D, et al. (2016b). Minimally Mutated HIV-1 Broadly Neutralizing Antibodies to Guide Reductionist Vaccine Design. PLoS Pathog 12, e1005815. [PubMed: 27560183]

Julg B, Pegu A, Abbink P, Liu J, Brinkman A, Molloy K, Mojta S, Chandrashekar A, Callow K, Wang K, et al. (2017). Virological Control by the CD4-Binding Site Antibody N6 in Simian-Human Immunodeficiency Virus-Infected Rhesus Monkeys. J Virol 91.

Kaplan HA, Welply JK, and Lennarz WJ (1987). Oligosaccharyl Transferase - the Central Enzyme in the Pathway of Glycoprotein Assembly. Biochimica Et Biophysica Acta 906, 161–173. [PubMed: 3297152]

Kasturi L, Eshleman JR, Wunner WH, and Shakineshleman SH (1995). The Hydroxy Amino-Acid in an Asn-X-Ser/Thr Sequon Can Influence N-Linked Core Glycosylation Efficiency and the Level of Expression of a Cell-Surface Glycoprotein. J Biol Chem 270, 14756–14761. [PubMed: 7782341]

Kwong PD, and Mascola JR (2012). Human Antibodies that Neutralize HIV-1: Identification, Structures, and B Cell Ontogenies. Immunity 37, 412–425. [PubMed: 22999947]

Liao HX, Lynch R, Zhou T, Gao F, Alam SM, Boyd SD, Fire AZ, Roskin KM, Schramm CA, Zhang Z, et al. (2013). Co-evolution of a broadly neutralizing HIV-1 antibody and founder virus. Nature 496, 469–476. [PubMed: 23552890]

Lin SC, Liu WC, Jan JT, and Wu SC (2014). Glycan masking of hemagglutinin for adenovirus vector and recombinant protein immunizations elicits broadly neutralizing antibodies against H5N1 avian influenza viruses. PLoS One 9, e92822. [PubMed: 24671139]

Marshall RD (1974). The nature and metabolism of the carbohydrate-peptide linkages of glycoproteins. Biochem Soc Symp, 17–26. [PubMed: 4620382]

Mascola JR, Stiegler G, VanCott TC, Katinger H, Carpenter CB, Hanson CE, Beary H, Hayes D, Frankel SS, Birx DL, et al. (2000). Protection of macaques against vaginal transmission of a pathogenic HIV-1/SIV chimeric virus by passive infusion of neutralizing antibodies. Nat Med 6, 207–210. [PubMed: 10655111]

Mastronarde DN (2005). Automated electron microscope tomography using robust prediction of specimen movements. Journal of Structural Biology 152, 36–51. [PubMed: 16182563]

McGuire AT, Gray MD, Dosenovic P, Gitlin AD, Freund NT, Petersen J, Correnti C, Johnsen W, Kegel R, Stuart AB, et al. (2016). Specifically modified Env immunogens activate B-cell precursors of broadly neutralizing HIV-1 antibodies in transgenic mice. Nat Commun 7, 10618. [PubMed: 26907590]

McGuire AT, Hoot S, Dreyer AM, Lippy A, Stuart A, Cohen KW, Jardine J, Menis S, Scheid JF, West AP, et al. (2013). Engineering HIV envelope protein to activate germline B cell receptors of broadly neutralizing anti-CD4 binding site antibodies. J Exp Med 210, 655–663. [PubMed: 23530120]

Mellquist JL, Kasturi L, Spitalnik SL, and Shakin-Eshleman SH (1998). The amino acid following an Asn-X-Ser/Thr sequon is an important determinant of N-linked core glycosylation efficiency. Biochemistry-Us 37, 6833–6837.

Nishimura Y, Gautam R, Chun TW, Sadjadpour R, Foulds KE, Shingai M, Klein F, Gazumyan A, Golijanin J, Donaldson M, et al. (2017). Early antibody therapy can induce long-lasting immunity to SHIV. Nature 543, 559–563. [PubMed: 28289286]

Novotny J, Handschumacher M, Haber E, Bruccoleri RE, Carlson WB, Fanning DW, Smith JA, and Rose GD (1986). Antigenic determinants in proteins coincide with surface regions accessible to large probes (antibody domains). Proc Natl Acad Sci U S A 83, 226–230. [PubMed: 2417241]

Onda M, Beers R, Xiang L, Nagata S, Wang QC, and Pastan I (2008). An immunotoxin with greatly reduced immunogenicity by identification and removal of B cell epitopes. Proc Natl Acad Sci U S A 105, 11311–11316. [PubMed: 18678888]

Pancera M, Zhou T, Druz A, Georgiev IS, Soto C, Gorman J, Huang J, Acharya P, Chuang GY, Ofek G, et al. (2014). Structure and immune recognition of trimeric pre-fusion HIV-1 Env. Nature 514, 455–461. [PubMed: 25296255]

Pantophlet R, Wilson IA, and Burton DR (2003). Hyperglycosylated mutants of human immunodeficiency virus (HIV) type 1 monomeric gp120 as novel antigens for HIV vaccine design. J Virol 77, 5889–5901. [PubMed: 12719582]

Pantophlet R, Wilson IA, and Burton DR (2004). Improved design of an antigen with enhanced specificity for the broadly HIV-neutralizing antibody b12. Protein Eng Des Sel 17, 749–758. [PubMed: 15542540]

Pegu A, Hessell AJ, Mascola JR, and Haigwood NL (2017). Use of broadly neutralizing antibodies for HIV-1 prevention. Immunol Rev 275, 296–312. [PubMed: 28133803]

Sampath S, Carrico C, Janes J, Gurumoorthy S, Gibson C, Melcher M, Chitnis CE, Wang R, Schief WR, and Smith JD (2013). Glycan masking of Plasmodium vivax Duffy Binding Protein for probing protein binding function and vaccine development. PLoS Pathog 9, e1003420. [PubMed: 23853575]

Saunders KO, Pegu A, Georgiev IS, Zeng M, Joyce MG, Yang ZY, Ko SY, Chen X, Schmidt SD, Haase AT, et al. (2015). Sustained Delivery of a Broadly Neutralizing Antibody in Nonhuman Primates Confers Long-Term Protection against Simian/Human Immunodeficiency Virus Infection. J Virol 89, 5895–5903. [PubMed: 25787288]

Scharf L, West AP Jr., Gao H, Lee T, Scheid JF, Nussenzweig MC, Bjorkman PJ, and Diskin R (2013). Structural basis for HIV-1 gp120 recognition by a germ-line version of a broadly neutralizing antibody. Proc Natl Acad Sci U S A 110, 6049–6054. [PubMed: 23524883]

Scheid JF, Mouquet H, Ueberheide B, Diskin R, Klein F, Oliveira TYK, Pietzsch J, Fenyo D, Abadir A, Velinzon K, et al. (2011). Sequence and Structural Convergence of Broad and Potent HIV Antibodies That Mimic CD4 Binding. Science 333, 1633–1637. [PubMed: 21764753]

Selvarajah S, Puffer B, Pantophlet R, Law M, Doms RW, and Burton DR (2005). Comparing antigenicity and immunogenicity of engineered gp120. J Virol 79, 12148–12163. [PubMed: 16160142]

Selvarajah S, Puffer BA, Lee FH, Zhu P, Li Y, Wyatt R, Roux KH, Doms RW, and Burton DR (2008). Focused dampening of antibody response to the immunodominant variable loops by engineered soluble gp140. AIDS Res Hum Retroviruses 24, 301–314. [PubMed: 18284327]

Sok D, Briney B, Jardine JG, Kulp DW, Menis S, Pauthner M, Wood A, Lee EC, Le KM, Jones M, et al. (2016). Priming HIV-1 broadly neutralizing antibody precursors in human Ig loci transgenic mice. Science 353, 1557–1560. [PubMed: 27608668]

Stewart-Jones GB, Soto C, Lemmin T, Chuang GY, Druz A, Kong R, Thomas PV, Wagh K, Zhou T, Behrens AJ, et al. (2016). Trimeric HIV-1-Env Structures Define Glycan Shields from Clades A, B, and G. Cell 165, 813–826. [PubMed: 27114034]

Steichen JM, Kulp DW, Tokatlian T, Escolano A, Dosenovic P, Stanfield RL, McCoy LE, Ozorowski G, Hu X, Kalyuzhniy O, et al. (2016). HIV Vaccine Design to Target Germline Precursors of Glycan-Dependent Broadly Neutralizing Antibodies. Immunity 45, 483–496. [PubMed: 27617678]

Tang G, Peng L, Baldwin PR, Mann DS, Jiang W, Rees I, and Ludtke SJ (2007). EMAN2: an extensible image processing suite for electron microscopy. J Struct Biol 157, 38–46. [PubMed: 16859925]

Thornton JM, Edwards MS, Taylor WR, and Barlow DJ (1986). Location of 'continuous' antigenic determinants in the protruding regions of proteins. EMBO J 5, 409–413. [PubMed: 2423325]

Tian M, Cheng C, Chen X, Duan H, Cheng HL, Dao M, Sheng Z, Kimble M, Wang L, Lin S, et al. (2016). Induction of HIV Neutralizing Antibody Lineages in Mice with Diverse Precursor Repertoires. Cell 166, 1471–1484 e1418. [PubMed: 27610571]

Tiller T, Busse CE, and Wardemann H (2009). Cloning and expression of murine Ig genes from single B cells. J Immunol Methods 350, 183–193. [PubMed: 19716372]

West AP Jr., Diskin R, Nussenzweig MC, and Bjorkman PJ (2012). Structural basis for germ-line gene usage of a potent class of antibodies targeting the CD4-binding site of HIV-1 gp120. Proc Natl Acad Sci U S A 109, E2083–2090. [PubMed: 22745174]

Wu X, Yang ZY, Li Y, Hogerkorp CM, Schief WR, Seaman MS, Zhou T, Schmidt SD, Wu L, Xu L, et al. (2010). Rational design of envelope identifies broadly neutralizing human monoclonal antibodies to HIV-1. Science 329, 856–861. [PubMed: 20616233]

Wu X, Zhang Z, Schramm CA, Joyce MG, Kwon YD, Zhou T, Sheng Z, Zhang B, O'Dell S, McKee K, et al. (2015). Maturation and Diversity of the VRC01-Antibody Lineage over 15 Years of Chronic HIV-1 Infection. Cell 161, 470–485. [PubMed: 25865483]

Wu X, Zhou T, Zhu J, Zhang B, Georgiev I, Wang C, Chen X, Longo NS, Louder M, McKee K, et al. (2011). Focused evolution of HIV-1 neutralizing antibodies revealed by structures and deep sequencing. Science 333, 1593–1602. [PubMed: 21835983]

Wyatt R, Sullivan N, Thali M, Repke H, Ho D, Robinson J, Posner M, and Sodroski J (1993). Functional and immunologic characterization of human immunodeficiency virus type 1 envelope glycoproteins containing deletions of the major variable regions. J Virol 67, 4557–4565. [PubMed: 8331723]

Zhou T, Georgiev I, Wu X, Yang ZY, Dai K, Finzi A, Kwon YD, Scheid JF, Shi W, Xu L, et al. (2010). Structural basis for broad and potent neutralization of HIV-1 by antibody VRC01. Science 329, 811–817. [PubMed: 20616231]

Zhou T, Lynch RM, Chen L, Acharya P, Wu X, Doria-Rose NA, Joyce MG, Lingwood D, Soto C, Bailer RT, et al. (2015). Structural Repertoire of HIV-1-Neutralizing Antibodies Targeting the CD4 Supersite in 14 Donors. Cell 161, 1280–1292. [PubMed: 26004070]

Zhou T, Zhu J, Wu X, Moquin S, Zhang B, Acharya P, Georgiev IS, Altae-Tran HR, Chuang GY, Joyce MG, et al. (2013). Multidonor analysis reveals structural elements, genetic determinants, and maturation pathway for HIV-1 neutralization by VRC01-class antibodies. Immunity 39, 245–258. [PubMed: 23911655]

Highlights:

- Engineering N-linked glycans onto eOD-GT8 improves its immunogenic specificity
- Added glycans mask binding to non-CD4bs antibodies but not VRC01-class antibodies
- Glycan masking focuses B cell response to CD4bs in human V_H1-2 mouse model
- The strategy enhances induction of VRC01-class antibody precursors in mice

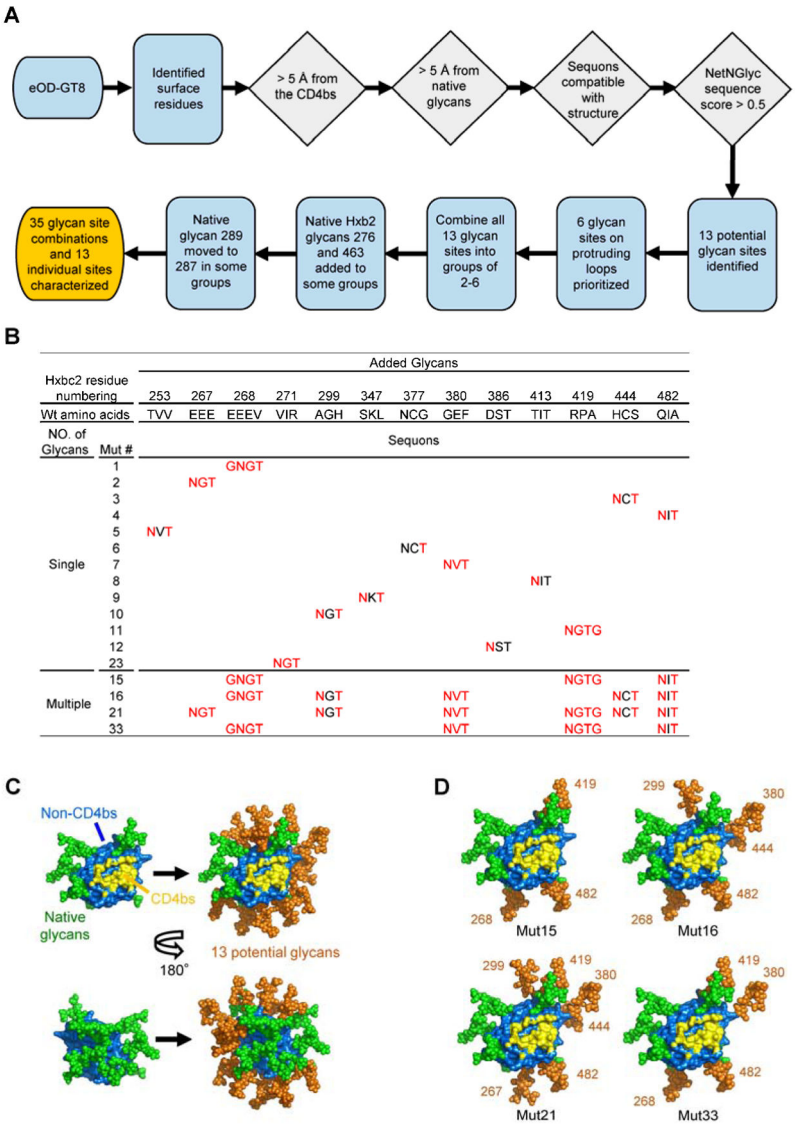

Figure 1. Addition of *N*-linked glycans to mask non-CD4bs epitopes on the eOD-GT8.

(A) Flow chart illustrating the strategy for adding new glycans to non-CD4bs surfaces of eOD-GT8. Gray diamonds indicate queries for surface residues; an affirmative answer resulted in progress to the next step. Blue rectangles indicate consecutive steps in the strategy and the orange rectangle indicates the end of the process. (B) Summary of added *N*-linked glycan positions on single mutants eOD-GT8-mut1-12 and 23 and multiple mutants eOD-GT8-mut15, 16, 21 and 33. Hxbc2 residue numbering and wildtype amino acid sequences and mutated amino acid sequences were shown. Mutated residues are highlighted in red. For labeling simplicity, the eOD-GT8 mutants are referred to by Mut# in this panel and subsequent figures. See also Table S1. (C) Surface representations of the eOD portion of eOD-GT8 showing the locations of predicted native glycans (green) and all 13 additional glycans modeled together (orange). The lower panels are rotated 180 degrees along the y-axis from the top panels. (D) Examples of combinations of glycan additions from four

selected designs modeled on eOD-GT8 with design numbers listed below each model. See also Figure S6.

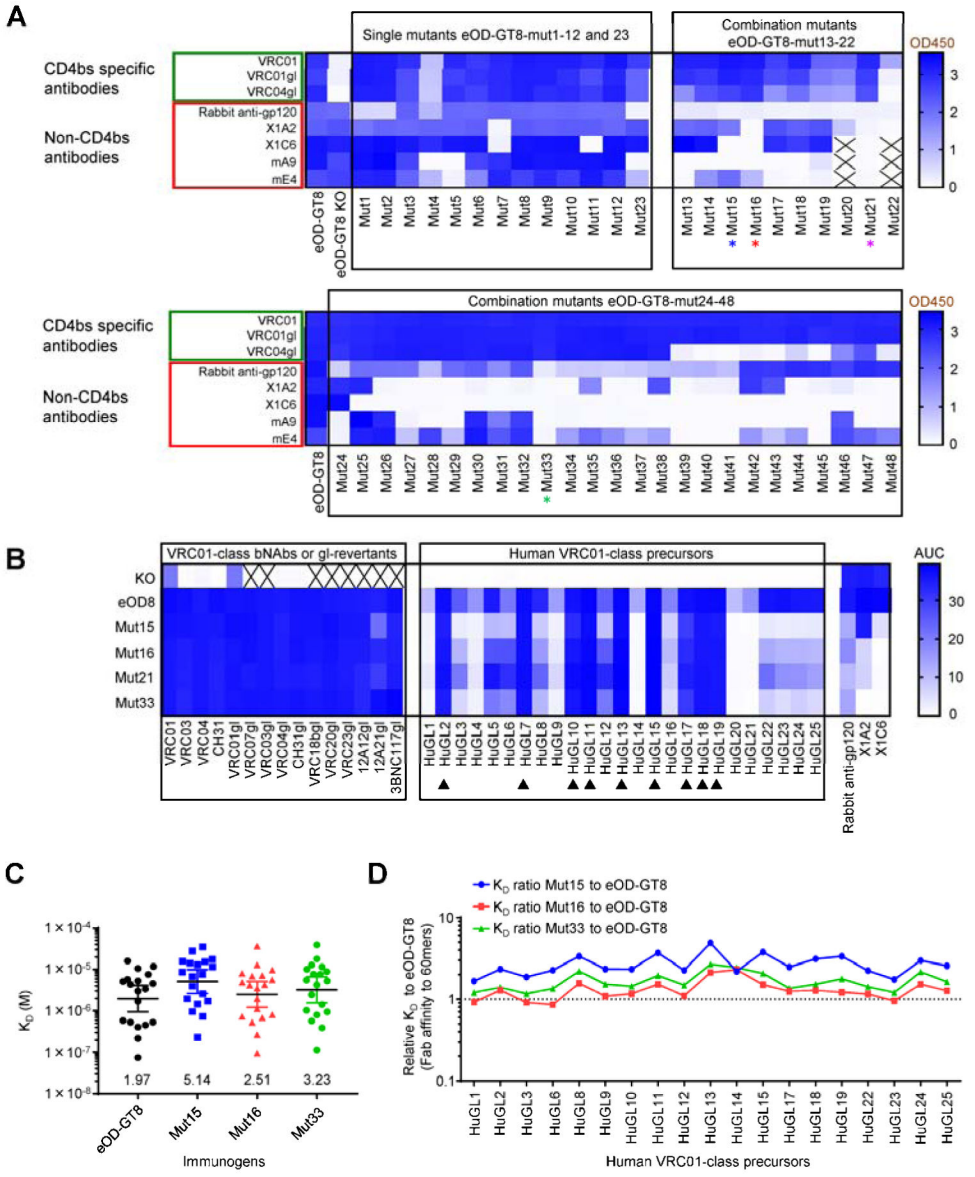

Figure 2. eOD-GT8 60mer glycan-masked mutants 15, 16, 21 and 33 have high affinity to CD4bs antibodies and low affinity to non-CD4bs antibodies.

(A) Heatmaps illustrating the ELISA binding (OD450 values in blue shading) of 48 different eOD-GT8 60mer mutants to CD4bs-specific mAbs (green box) and non-CD4bs antibodies or serum (red box). Four mutants, marked by asterisks, bound with lowest affinity to non-CD4bs antibodies while they retained high affinity for CD4bs-specific mAbs. X indicates assay not performed. (B) Heatmap displaying the ELISA binding (area under the curve (AUC), in blue shading) of eOD-GT8 (eOD8), eOD-GT8 KO (KO) and glycan mutants eOD-GT8-mut15, 16, 21 and 33 60mer to a panel of CD4bs-specific VRC01-class antibodies and germline revertant antibodies, and 25 human VRC01-class IgG precursors (HuGL1-25). High affinity binders (K_D to eOD-GT8 < 3 μM) are marked with arrowheads. Rabbit-anti-gp120 serum and two non-CD4bs mAbs were used as controls. (C) Scatter plot showing SPR K_D values (Geometric mean±95%CI) for the recognition of eOD-GT8 60mer

and eOD-GT8-mut15, 16 and 33 60mer by 19 HuGL Fabs (also shown in the x-axis of panel D). The results shown represent one of two independent experiments with similar results. (D) Plot illustrating the ratio of eOD-GT8 mutant K_Ds (from panel C) relative to eOD-GT8 K_D for 19 HuGL Fabs. Dashed line indicates a ratio of 1.0. The asterisks in (A) and the affinity data in (C-D) are colored-coded as follows: eOD-GT8-mut15, blue; eOD-GT8-mut16, red; eOD-GT8-mut21, magenta and eOD-GT8-mut33, green. See also Figure S1.

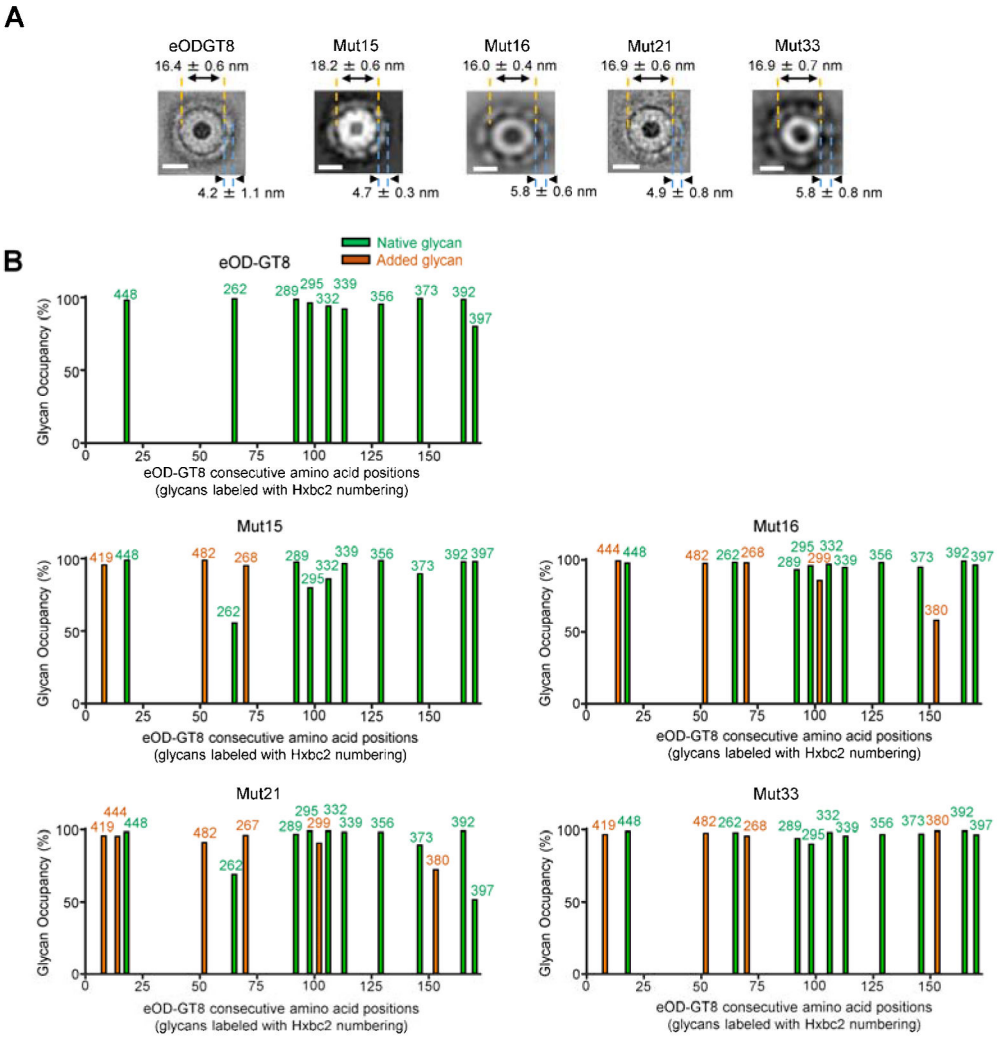

Figure 3. Electron microscopy and glycan occupancy analysis confirmed particle formation and glycan addition for glycan-masked eOD-GT8 mutants 15, 16, 21 and 33 60mers

(A) Typical 2D-averaged negative-stained electron microscopy images of the parental and mutant eOD-GT8 60mer nanoparticles. From left to right, the number of particles used for each 2D-average was 97, 35, 127, 51, and 14 respectively. Average dimensions are shown with standard deviations and white scale bars indicate 10 nms. (B) Glycan occupancy for parental and mutant eOD-GT8 immunogens as detected by LC-MS. The x-axis indicates the consecutive amino acid positions on the circularly permutated eOD-GT8 immunogen. The green bars (native) and orange bars (added) indicates the percentage glycan occupancy for each of the glycosylated positions (labeled with HxBc2 residue positions). The results shown are from one experiment and eOD-GT8 mutants 15 and 16 results were each averaged from two separate lots of protein (See also Figure S2).

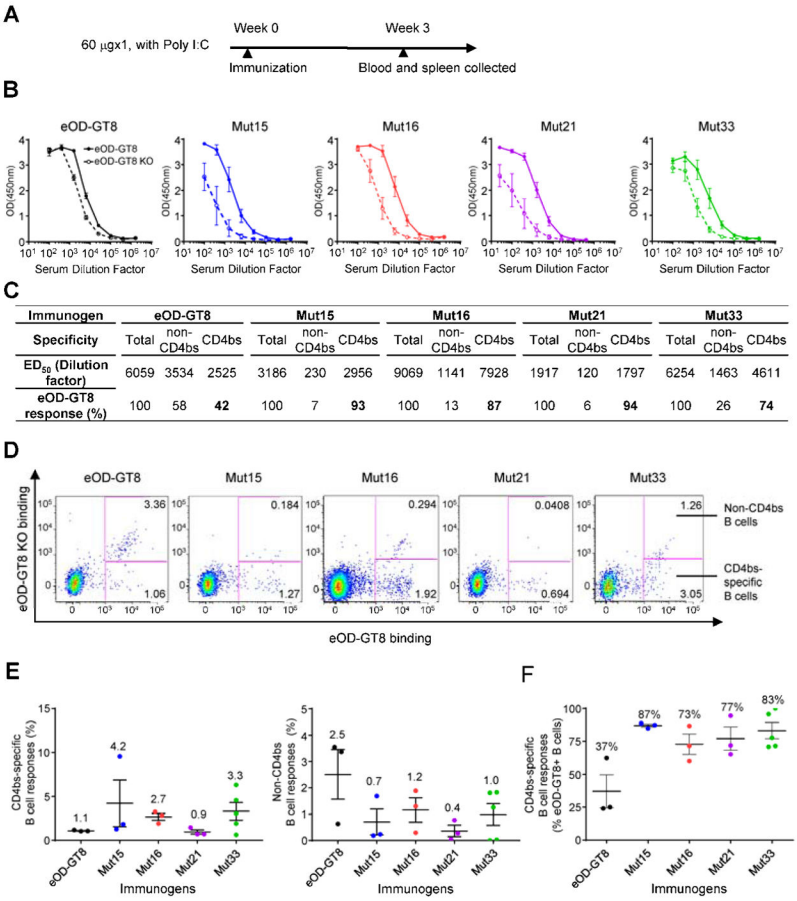

Immunogen	eOD-GT8			Mut15			Mut16			Mut21			Mut33		
Specificity	Total	non-CD4bs	CD4bs	Total	non-CD4bs	CD4bs	Total	non-CD4bs	CD4bs	Total	non-CD4bs	CD4bs	Total	non-CD4bs	CD4bs
ED_{50} (Dilution factor)	6059	3534	2525	3186	230	2956	9069	1141	7928	1917	120	1797	6254	1463	4611
eOD-GT8 response (%)	100	58	**42**	100	7	**93**	100	13	**87**	100	6	**94**	100	26	**74**

Figure 4. Glycan-masking of eOD-GT8 60mer immunogens improved the CD4bs-specific antibody response.

(A) Immunization scheme for the first experiment (n = 3 for eOD-GT8, Mut15, Mut16, Mut21; n = 5 for Mut33). (B) ELISA plots (mean±SEM) showing recognition of eOD-GT8 (solid lines) and eOD-GT8 KO (dashed lines) by sera elicited by the indicated immunogens (color-coded as in Figure 2). (C) Quantification of ELISA data from (B) showing the ED_{50} (dilution factors) and percent sera responses for each immunogen. (D) Representative flow cytometry plots for IgG^+ B cells from immunized IGHV1-2*02 KI mice. The percentages of CD4bs-specific IgG^+ B cells (eOD-$GT8^+$; eOD-GT8 KO^-) and non-CD4bs B cells (eOD-$GT8^+$; eOD-GT8 KO^+) are indicated in the respective right quadrants of each plot. (E) Scatter - plots (mean ±SEM) showing the percent CD4bs-specific (left) and non-CD4bs (right) IgG^+ B cells relative to total IgG^+ population. (F) Scatter plot (mean ±SEM) showing the percent of CD4bs-specific IgG^+ B cells relative to eOD-$GT8^+$ B cells. Dots in (E-F) represent individual mice color-coded as in Figure 2. See also Figures S3-S4 and Tables S2, S5-S6.

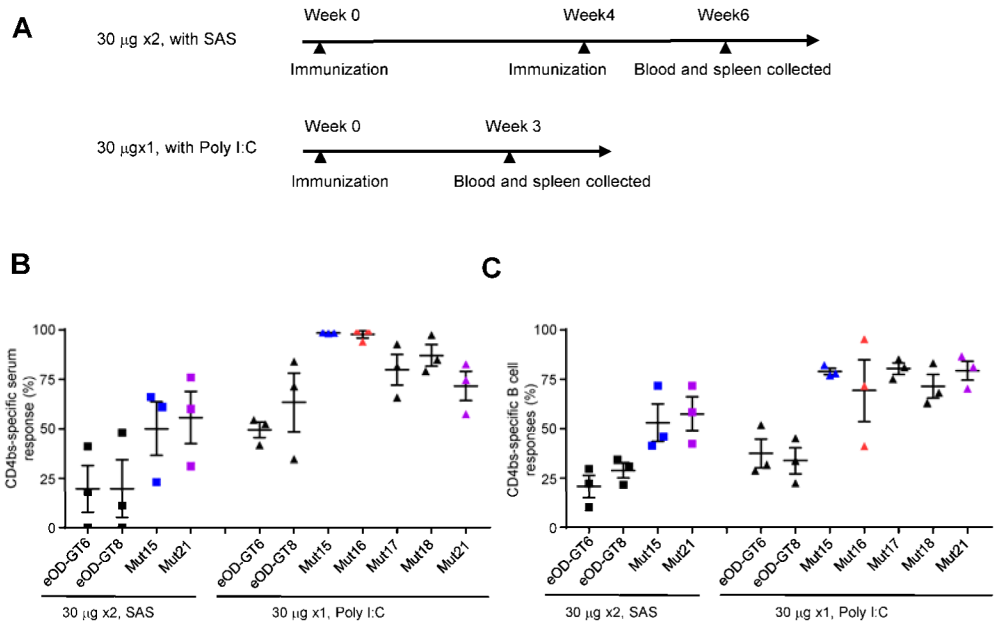

Figure 5. Additional immunization regimens confirmed that glycan-masking of eOD-GT8 improved the CD4bs-specific antibody response.

(A) Immunization schema for the second and third experiments ($n = 3$). (B-C) Scatter plots (mean ±SEM) showing the percent CD4bs-specific sera responses (B) and percent CD4bs-specific B cells (relative to the total antigen-specific populations) (C) elicited by the indicated immunizations. Data points from the second and third immunization studies are depicted by squares and triangles respectively. See also Figure S3 and Tables S3-S6.

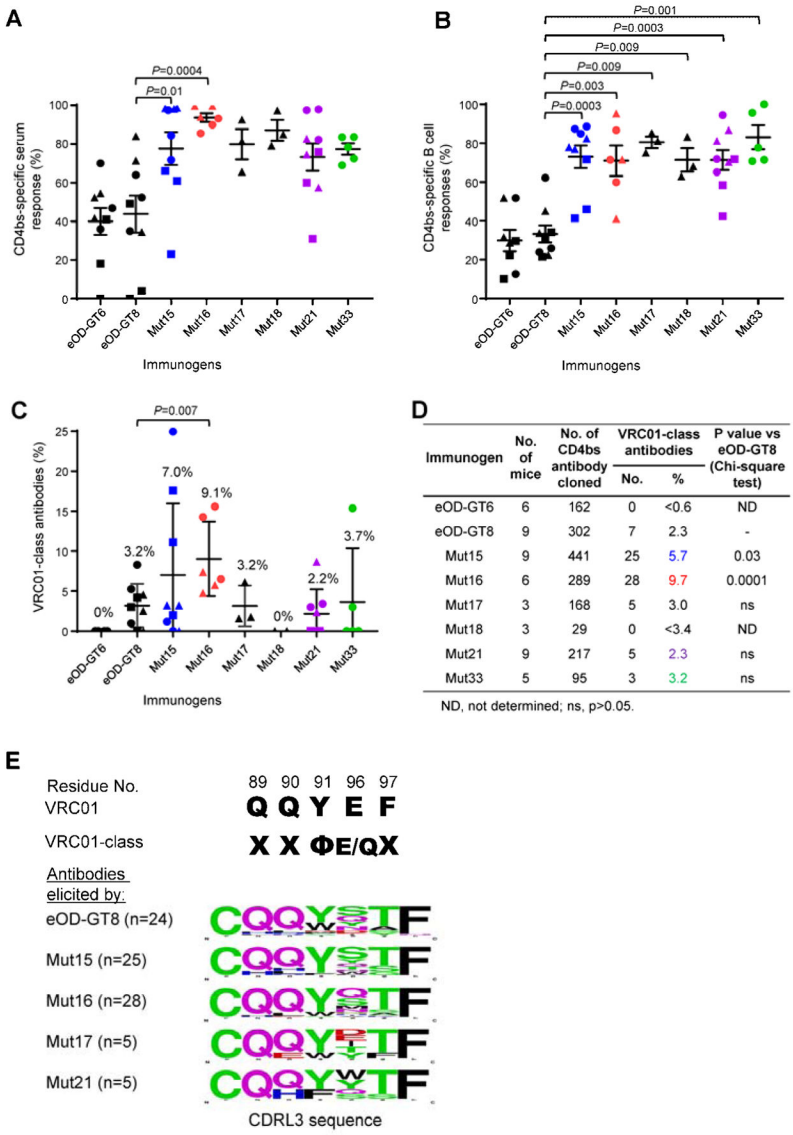

Immunogen	No. of mice	No. of CD4bs antibody cloned	VRC01-class antibodies		P value vs eOD-GT8 (Chi-square test)
			No.	%	
eOD-GT6	6	162	0	<0.6	ND
eOD-GT8	9	302	7	2.3	-
Mut15	9	441	25	5.7	0.03
Mut16	6	289	28	9.7	0.0001
Mut17	3	168	5	3.0	ns
Mut18	3	29	0	<3.4	ND
Mut21	9	217	5	2.3	ns
Mut33	5	95	3	3.2	ns

ND, not determined; ns, p>0.05.

Figure 6. Compilation of three immunization studies confirmed that glycan-masking of eOD-GT8 improved the CD4bs-specific antibody response and enhanced elicitation of VRC01-class antibodies.

(A-C) present the combined data from Figures 4 and 5, grouped by immunogen. Scatter plots (mean±SEM) show the percent CD4bs-specific sera responses (A), the percent CD4bs-specific B cells (relative to the total antigen-specific B cell populations) (B) and frequencies of VRC01-class antibodies (C) elicited by the indicated immunogens. In (C), the mean percentages are shown above each respective immunogen. For (A-C) each point represents a mouse, with data points from the first, second and third immunization studies depicted by circles, squares and triangles respectively color-coded as in Figure 2. *P*-values (unpaired Mann-Whitney) less than 0.01 are shown after confirming an overall nonparametric ANOVA Kruskal-Wallis test gave a *p*-value of less than 0.05. ns, nonsignificant ($p > 0.01$). (D) Tabulated data quantifying the VRC01-class antibodies identified from B cells of all mice studied, grouped by immunogen. The percentages of VRC01-class antibodies are color-

coded by immunogen. (E) Sequence conservation of 5-amino acid CDRL3 loops of elicited VRC01-class antibodies. X refers to any amino acid and Φ refers to hydrophobic residues. Sequence Logo plots illustrate the amino acids distributions at each CDRL3 position in VRC01-class antibodies elicited by the indicated immunogens. The relative height of each letter denotes the frequency for observing that amino acid at that position. eOD-GT8- mut33 60mer was not shown due to low numbers of isolated sequences (3 in total). See also Figures S3, S5-S6 and Tables S2-S6.